HOKKAIDO UNIVERSITY

Title	Mapping the band structure of a surface phononic crystal
Author(s)	Maznev, A. A.; Wright, O. B.; Matsuda, O.
Citation	New Journal of Physics, 13, 013037 https://doi.org/10.1088/1367-2630/13/1/013037
Issue Date	2011-01
Doc URL	https://hdl.handle.net/2115/45149
Type	journal article
File Information	NJP13_013037.pdf

Hokkaido University Collection of Scholarly and Academic Papers : HUSCAP

New Journal of Physics
The open-access journal for physics

Mapping the band structure of a surface phononic crystal

A A Maznev[1,2,3], O B Wright[1] and O Matsuda[1]

[1] Division of Applied Physics, Graduate School of Engineering, Hokkaido University, Sapporo 060-8628, Japan

[2] Department of Chemistry, Massachusetts Institute of Technology, Cambridge, MA 02139, USA

E-mail: maznev@mit.edu

New Journal of Physics **13** (2011) 013037 (11pp)
Received 26 July 2010
Published 25 January 2011
Online at http://www.njp.org/
doi:10.1088/1367-2630/13/1/013037

Abstract. We map the band structure of surface acoustic modes of a periodic array of copper lines embedded in a SiO_2 film on a silicon substrate by means of the laser-induced transient grating technique. A detailed map of the lowest sheet of the $\omega(\mathbf{k})$ surface and partial maps of two higher-order sheets are obtained. We discuss the topology of the $\omega(\mathbf{k})$ surface and explain how it arises from the Rayleigh and Sezawa modes of the film/substrate system. In the vicinity of the bandgap formed at the Brillouin zone boundary, the first and second dispersion sheets take the form of a saddle and a bowl, respectively, in agreement with a weak perturbation model. The shape of the third dispersion sheet, however, appears to defy expectations based on the perturbation approach. In particular, it contains minima located off the symmetry directions, which implies the existence of zero group velocity modes with an obliquely directed wavevector.

Contents

1. Introduction 2
2. Experiment 2
3. Results and discussion 4
4. Conclusions 9
Acknowledgments 10
References 10

[3] Author to whom any correspondence should be addressed.

© IOP Publishing Ltd and Deutsche Physikalische Gesellschaft

1. Introduction

Studies of the propagation of acoustic waves in periodic structures go back over half a century [1] and have resulted in many widely used applications, particularly in the area of surface acoustic wave (SAW) devices [2]. Recent years have seen an explosion of activity in this field, with the focus on new phenomena found in two-dimensional (2D) and 3D structures, such as complete bandgaps, and the term 'phononic crystals' is now broadly used to define the acoustics of periodic structures [3]. SAWs on periodically structured surfaces that can be termed 'surface phononic crystals' (SPCs) have also attracted increasing attention both within and outside the traditional SAW device field [4]–[13].

The main characteristic of an SPC is the shape of the dispersion bands that form surfaces $\omega(\mathbf{k})$ in a 3D space. Experimental studies of SPCs published to date only involve measurements of *dispersion curves* along limited selected directions of the acoustic wavevector [5, 11, 14]. Accurate mapping of the *dispersion surface* in 3D ω, k_x, k_y space, where ω is the angular frequency and k_x, k_y are components of the 2D wavevector $\mathbf{k}$, would therefore obviously be desirable for the investigation of SPCs.

Since solid surfaces are amply accessible for optical measurements, non-contact laser-based methods are particularly attractive for studying SPCs. An early version of the optical pump–probe technique [15] makes use of a femtosecond pulse illuminating a wide area compared to the SPC period to excite surface vibrations, which are detected by a variably delayed probe pulse. This method has been applied to both 1D and 2D SPCs [9, 10, 15], but has the disadvantage that only a single point $\mathbf{k} = 0$ in the reduced Brillouin zone (BZ) is accessible. Another version of the femtosecond pump–probe setup [8, 13] combines a point-like excitation and a scanning point-like probe that allows 2D imaging of the acoustic field. This method proved to be capable of accessing the full $\omega(\mathbf{k})$ surface [8], but the resolution of the measurements on the frequency axis was limited by the fact that only discrete points corresponding to multiples of the laser repetition rate of 76 MHz were accessible. The method produced some intriguing constant frequency cross-sections of the dispersion surface but fell short of resolving the details of the band structure.

In this work, we use an alternative technique for mapping $\omega(\mathbf{k})$ based on the laser-induced transient grating method [5, 11, 12], in which two optical excitation pulses form an interference pattern at the sample surface, thus precisely defining the wavevector of the excited SAWs. The magnitude and the direction of the wavevector can easily be varied, thus allowing direct mapping of the $\omega(\mathbf{k})$ surface. We investigate the band structure of a relatively simple 1D SPC similar to that studied in [8]. The higher data quality compared to the previous work allows us to reconstruct the shape of the $\omega(\mathbf{k})$ surface and gain better understanding of the main topological features of the band structure.

2. Experiment

The sample used in this work is identical to that of [8], except that no gold coating was used. A schematic cross-section of the sample is shown in figure 1(a). Copper lines are embedded in a 0.8 μm thick SiO_2 film on a (100) silicon substrate. The substrate of thickness 720 μm can be considered semi-infinite for the purposes of this study. The copper linewidth is 2 μm and the structure period is $d = 4\,\mu$m. The lines are aligned along the [011]-axis of the Si substrate. The lateral dimensions of the line array pattern are $3 \times 3\,\text{mm}^2$.

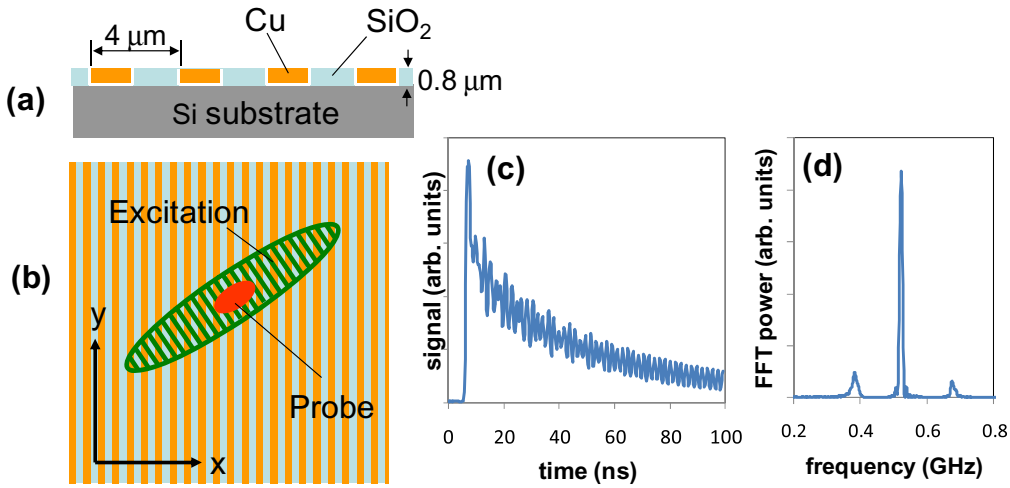

Figure 1. (a) Cross-section of the sample and (b) top view showing the laser spot (not to scale); (c) an example of a signal waveform and (d) the frequency spectrum of the acoustic oscillations. The data were taken with the excitation grating wavevector of 0.97 μm^{-1} (grating period 6.5 μm) perpendicular to the Cu lines.

The transient grating apparatus with optical heterodyne detection has been described elsewhere [16]. In summary, two excitation pulses derived from a single laser (pulse duration 0.5 ns, wavelength 532 nm and total energy at the sample $\sim$1 μJ) form a spatially periodic interference pattern at the sample surface. Absorption of the excitation light followed by rapid thermal expansion generates counter-propagating acoustic modes at the wavevector defined by the periodicity of the excitation grating. Detection of the surface ripples associated with surface acoustic modes is performed via diffraction of the quasi-cw probe beam (wavelength 830 nm and power at the sample $\sim$100 mW) focused at the center of the excitation pattern. The diffraction signal amplified via optical heterodyning is detected with a fast photodiode and fed to a digital oscilloscope, giving an effective bandwidth $\sim$1 GHz for the detection electronics. The excitation spot size is $300 \times 50\,\mu\text{m}^2$ and the probe spot size is $50 \times 25\,\mu\text{m}^2$. The location of the excitation and the probe laser beams at the sample surface is schematically shown in figure 1(b).

Figure 1(c) shows an example of a signal waveform. The initial sharp rise indicates the moment when the excitation pulse strikes the sample. High-frequency oscillations are due to surface acoustic modes, whereas the slowly decaying component is the contribution of the 'thermal grating' associated with the periodic temperature profile. The Fourier spectrum of the acoustic oscillations reveals the presence of three surface acoustic modes observed within the frequency bandwidth of the experiment. As we will see, these three modes correspond to the three lowest sheets of the $\omega(\mathbf{k})$ surface. The observed decay of the oscillations is not caused by acoustic damping, but rather by the fact that the signal is only observed while counter-propagating wavepackets pass through the probe spot. Thus, the frequency resolution of the technique is determined by the laser spot size and the group velocity of the acoustic waves. In the vicinity of the bandgaps, where the group velocity approaches zero, the oscillations are particularly long lived and yield narrow peaks exemplified by the central peak in figure 1(d), which, as we shall see, corresponds to a saddle point of $\omega(\mathbf{k})$. In practice, the 100 ns time window used for

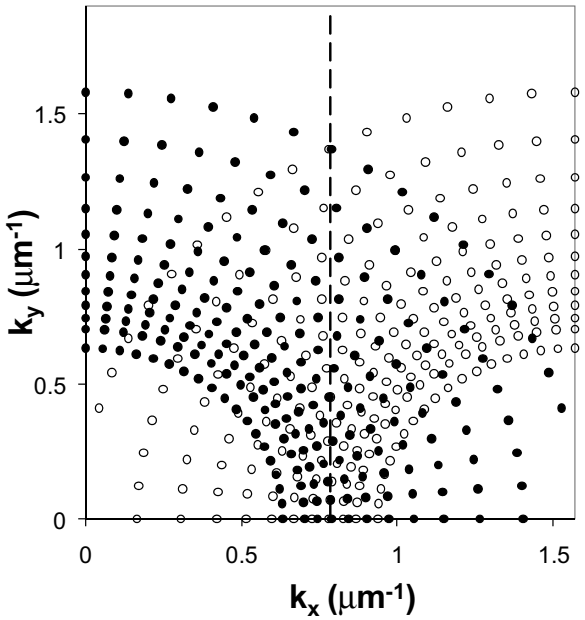

Figure 2. Measured points in **k**-space (closed circles) and symmetrically equivalent points (open circles). The vertical dashed line marks the BZ boundary.

the measurements sets a lower bound for the peak width at about 5 MHz; if needed, further improvement of the frequency resolution in the vicinity of the bandgaps could be achieved by expanding the time window. The precision (reproducibility) of the measurements of the position of the frequency peaks was typically better than 0.1 MHz [16].

In order to map the $\omega(\mathbf{k})$ surface, one needs to vary both the magnitude and the direction of the wavevector. The experimental setup allowed us to vary the wavenumber within a set of 12 fixed values in the range 0.63–1.58 μm^{-1} (which corresponds to the range 4–10 μm in the grating period). The direction of the wavevector was varied by rotating the sample in 5° steps. Figure 2 shows the array of measured points in (k_x, k_y) space. Due to the periodicity of the structure, the acoustic mode dispersion in **k**-space is also periodic along k_x, with the period equal to the 'wavenumber' of the Cu line pattern $q = 2\pi/d$. Due to the symmetry of the sample, there is also reflection symmetry with respect to both the $k_x = 0$ and $k_y = 0$ axes. From the periodicity and symmetry with respect to $k_x = 0$, it follows that $\omega(\mathbf{k})$ should also be symmetric with respect to the BZ boundary $k_x = k_B = \pi/d$. This fact helps us to get a reasonable coverage of the BZ even with the limited wavenumber range. Indeed, one can see that the lowest wavenumber of 0.63 μm^{-1} results in a large 'hole' at the center of the BZ. However, this 'hole' is covered by symmetrically equivalent points obtained from the measurements at large excitation wavenumbers.

3. Results and discussion

The measured 3D map of the $\omega(\mathbf{k})$ surface is presented in figure 3. The surface was produced using a triangle-based linear interpolation algorithm in the MathLab software package that yields a surface always passing through the data points. As mentioned above, in the frequency range below 1 GHz, the dispersion surface comprises three sheets.

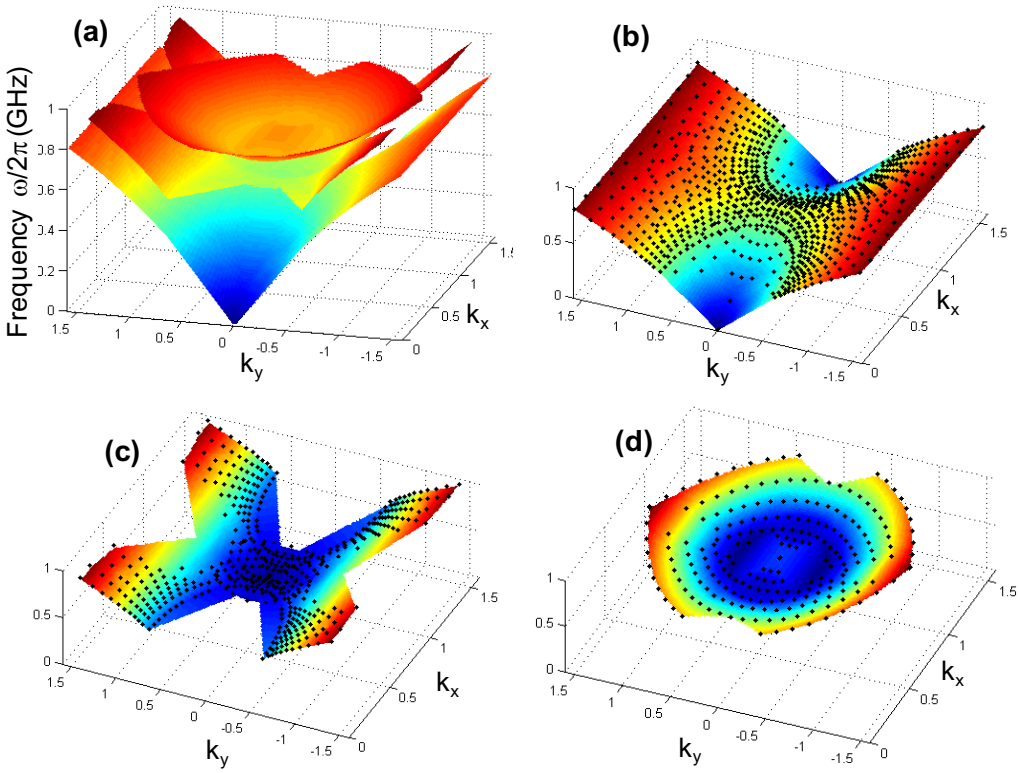

Figure 3. Measured 3D map of the acoustic frequency versus wavevector surface with the three lowest dispersion sheets shown (a) together and (b–d) separately. Solid symbols correspond to experimental data (including points obtained from the measured ones by symmetry transformations). The point $\mathbf{k} = 0$, $\omega = 0$, which is not experimentally accessible, has been added to the lowest dispersion sheet based on the known fact that the lowest mode does not have a low-frequency cut-off since at low frequencies it should transform into the Rayleigh wave of the substrate. Wavevector components k_x and k_y are expressed in $\mu\mathrm{m}^{-1}$.

The first (lowest) sheet yielded the most complete map within the covered wavevector range; for the other two sheets, we only obtained partial maps since the corresponding peaks in the spectrum were below the noise level at some points in **k**-space. The first sheet has the simplest shape, with a saddle point located at the BZ boundary at $k_x = k_\mathrm{B}$ and $k_y = 0$. The more complicated shape of the second and third dispersion sheets is discussed below. Parts of the measured dispersion surfaces belong to pseudo-surface or 'leaky' modes coupled to bulk waves in the substrate [17]. For an isotropic substrate, all modes located above the cone $\omega = c_\mathrm{t}|\mathbf{k}|$ in the reduced BZ, where c_t is the transverse velocity of the substrate, should be leaky. For an anisotropic substrate, c_t should be replaced by the angle-dependent limiting velocity [18] whose value is within the range of anisotropic quasi-transverse velocities of the substrate. For the purposes of the study of the shape of the dispersion surface, we will make no distinction between leaky waves and true surface modes since the attenuation of the leaky waves only affects the width of measured spectral peaks [11].

Let us start the discussion of the topology of the $\omega(\mathbf{k})$ surface with a study of its cross-sections with the $k_x = 0$ and $k_y = 0$ planes (i.e. the dispersion curves measured along the

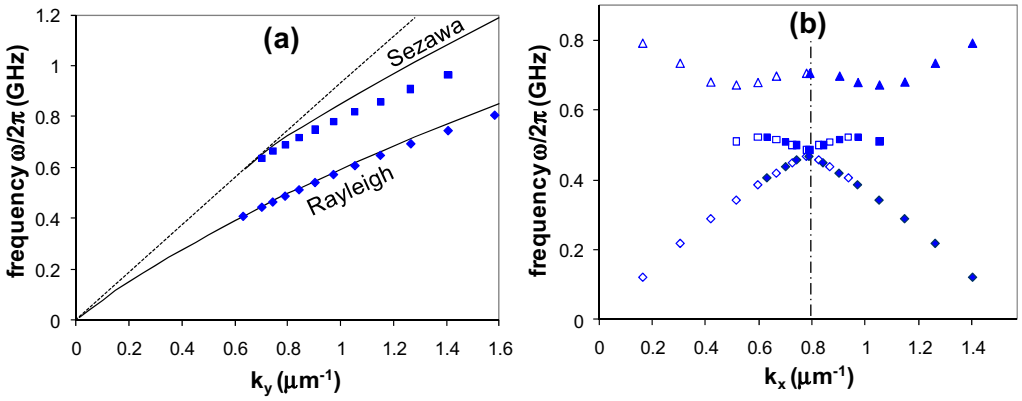

Figure 4. Measured acoustic dispersion curves (a) along the y-axis and (b) along the x-axis. Diamonds, squares and triangles refer to the three sheets of $\omega(\mathbf{k})$. Solid symbols correspond to the experimentally measured points, whereas open symbols are obtained from symmetry transformations. Solid lines in (a) are obtained from calculations based on an effective medium model for the Cu/SiO_2 layer. The dotted line in (a) corresponds to vertically polarized bulk transverse waves in the Si substrate. The dashed-dotted line in (b) marks the BZ boundary $k_x = k_B$.

y- and x-directions, respectively) presented in figure 4. It is apparent that the two modes in the $k_x = 0$ cross-section correspond to the familiar Rayleigh and Sezawa modes of a film/substrate structure, with the Sezawa mode appearing from under the bulk transverse threshold [19].

It is instructive to compare measured dispersion curves with an effective medium model treating the structure as a homogeneous layer with effective elastic properties. To calculate the effective properties of a periodic layered structure comprised of Cu and SiO_2 layers, we used effective-medium equations from [20], properties of chemical-vapor-deposited SiO_2 from [21] and properties of polycrystalline Cu from [22]. The effective medium has transversely isotropic symmetry and is characterized by the effective density of 5565 kg m^{-3} and five elastic constants [20]; however, in the analysis of acoustic waves with both propagation and polarization directions contained in the plane perpendicular to the direction of periodicity, only two elastic constants are involved, and those can be expressed in terms of the effective longitudinal and transverse velocities 4686 and 2533 m s^{-1}, respectively. We subsequently used a standard method [19] for calculating velocities of guided modes for a homogeneous layer on a semi-infinite elastically anisotropic Si substrate.

For the effective medium model [20] to be accurate, the period of the structure should be small compared to both the acoustic wavelength and the thickness of the layer. Although neither of these requirements is met, figure 4(a) shows that at longer wavelengths the calculated dispersion curves nearly agree with the measured ones.

The cross-section with the $k_y = 0$ plane shown in figure 4(b) reveals a more intricate shape that was investigated in detail for similar structures in [11, 23]. The dispersion bands of a periodic structure result from 'zone-folding' of the Rayleigh and Sezawa dispersion curves and the formation of avoided crossing bandgaps, as schematically shown in figure 5. The Rayleigh–Rayleigh and Sezawa–Sezawa crossings result in bandgaps located either at the boundary or at the center of the BZ, whereas Rayleigh–Sezawa crossings result in bandgaps

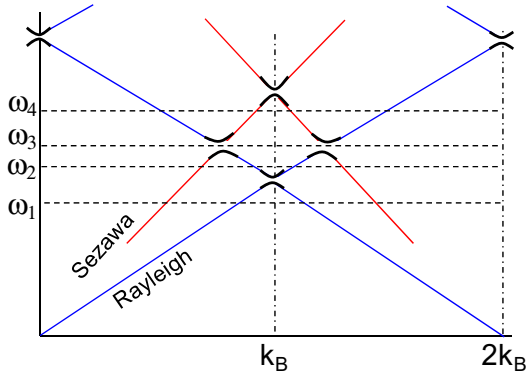

Figure 5. Schematic diagram of the $k_y = 0$ cross-section of the $\omega(\mathbf{k})$ surface in the limit of weak periodicity. 'Avoided crossing' bandgaps lead to the formation of dispersion sheets composed of sections of the original Rayleigh (blue) and Sezawa (red) dispersion cones. The horizontal dashed lines approximately correspond to isofrequency cross-sections presented in figure 7 below.

inside the BZ. The original dispersion curves of the Rayleigh and Sezawa modes thus combine and separate into sheets of the $\omega(\mathbf{k})$ surface of the periodic structure. The lowest sheet is formed by the Rayleigh-like waves, whereas the second and third sheets are composed of parts of both the Rayleigh and the Sezawa bands. As can be seen in figure 3(b), in experiment the bandgap resulting from the Rayleigh–Sezawa crossing is much greater than the one formed at the BZ boundary. This has been explained in [23] as being due to the structure of displacement patterns in the eigenmodes formed by counter-propagating Rayleigh- and Sezawa-like waves.

Let us consider what happens to the $\omega(\mathbf{k})$ surface in 3D when the bandgaps are formed. In the absence of periodicity, dispersion sheets of the Rayleigh and Sezawa modes have a nearly conical shape. Bandgap formation in the case of weak periodicity can be described using the general expression for the frequencies of weakly interacting oscillators [24],

$$\omega_{1,2} = \frac{1}{2}\left[(\omega_{01} + \omega_{02}) \pm \sqrt{(\omega_{01} - \omega_{02})^2 + \Delta^2}\right], \tag{1}$$

where ω_{01} and ω_{02} are the frequencies of the unperturbed oscillators and Δ is the width of the bandgap. For example, in the vicinity of the first bandgap formed at the zone boundary $\mathbf{k}_\mathrm{B} = (k_\mathrm{B}, 0)$, the frequencies of the unperturbed counter-propagating Rayleigh waves are given by

$$\omega_{01,02} = \omega_0 \pm v(k_x - k_\mathrm{B}) + ck_y^2, \tag{2}$$

where ω_0 and v are the Rayleigh wave frequency and group velocity at $\mathbf{k} = \mathbf{k}_\mathrm{B}$, and the constant c is equal to $c = v/2k_\mathrm{B}$ in the isotropic case, but may be modified due to the elastic anisotropy of the substrate. Equation (1) now takes the form

$$\omega_{1,2} = \omega_0 + ck_y^2 \pm \sqrt{v^2\,(k_x - k_\mathrm{B})^2 + \Delta^2/4}. \tag{3}$$

The '+' sign in equation (3) yields a parabolic minimum at $\mathbf{k}_\mathrm{B}$, whereas the '−' sign yields a saddle-shaped surface. The transformation of intersecting conical surfaces into an elliptical paraboloid and a saddle is illustrated with an example in figure 6.

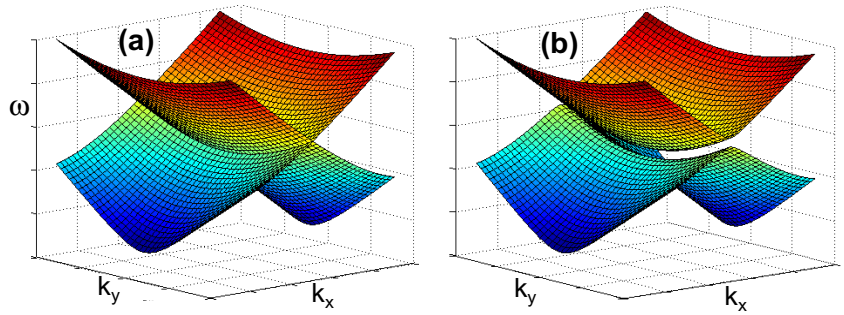

Figure 6. (a) Intersecting conical dispersion sheets corresponding to counter-propagating Rayleigh waves in the limit of vanishing periodicity; (b) the formation of a saddle and an elliptical paraboloid as a result of the avoided crossing described by equation (3).

We can now trace the formation of the three dispersion sheets out of the original Rayleigh and Sezawa cones with the help of figure 7(a), (b), which schematically shows constant frequency cross-sections of the $\omega(\mathbf{k})$ surface. The four cross-sections shown correspond to the four frequencies indicated in figure 5: below and above the first bandgap, inside and above the second bandgap. One can see how the dispersion sheets are composed of sections of the original conical surfaces. When two cones 'touch' each other, a bandgap arises, with a saddle at the bottom and a parabolic minimum at the top. Thus, the first dispersion sheet has a saddle point at the BZ boundary; the second sheet yields a parabolic minimum at the BZ boundary and saddles inside the BZ, whereas the third sheet forms a saddle at the BZ boundary and parabolic minima inside the BZ. When the frequency is inside the bandgap (ω_3 in figure 7), the isofrequency cross-section also forms a gap, indicating that there are no propagating modes below some critical value of $|k_y|$.

Figure 7(c) shows the isofrequency cross-sections of the experimentally measured dispersion sheets loosely corresponding to the model cross-sections in figure 7(b) (the latter drawn by hand rather than calculated). Qualitative agreement between figures 7(b) and (c) can clearly be seen for the first mode as well as for the partial data available for the second mode. This agreement can also be seen in figure 8, which shows detailed maps of the dispersion sheets: the first mode has a saddle point at the BZ boundary $k_B = 0.79\,\mu\mathrm{m}^{-1}$, whereas the second mode has a parabolic minimum at the BZ boundary and two saddles either side of it.

However, the measured shape of the third dispersion sheet shown in figure 8(c) differs from the expectations based on the weak perturbation model. Instead of a saddle point, the measured surface yields a maximum at $\mathbf{k}_B = (k_B, 0)$, and unexpected deep minima are formed above and below it at $|k_y| \sim 0.4\,\mu\mathrm{m}^{-1}$. Clearly, we are not in the 'weak perturbation' limit here, as the gap between the second and third dispersion sheets is quite large. However, the very possibility for the $\omega(\mathbf{k})$ surface to have a minimum located off the symmetry axis $k_y = 0$ is intriguing. In particular, this implies the existence of a zero group velocity mode with the reduced wavevector at an angle of $\sim 30^\circ$ to the direction of periodicity of the structure. The existence of off-axis zero group velocity waves in a 1D periodic structure is not intuitive: the naïve expectation is that a 1D structure would only be capable of confining waves propagating in the direction of periodicity.

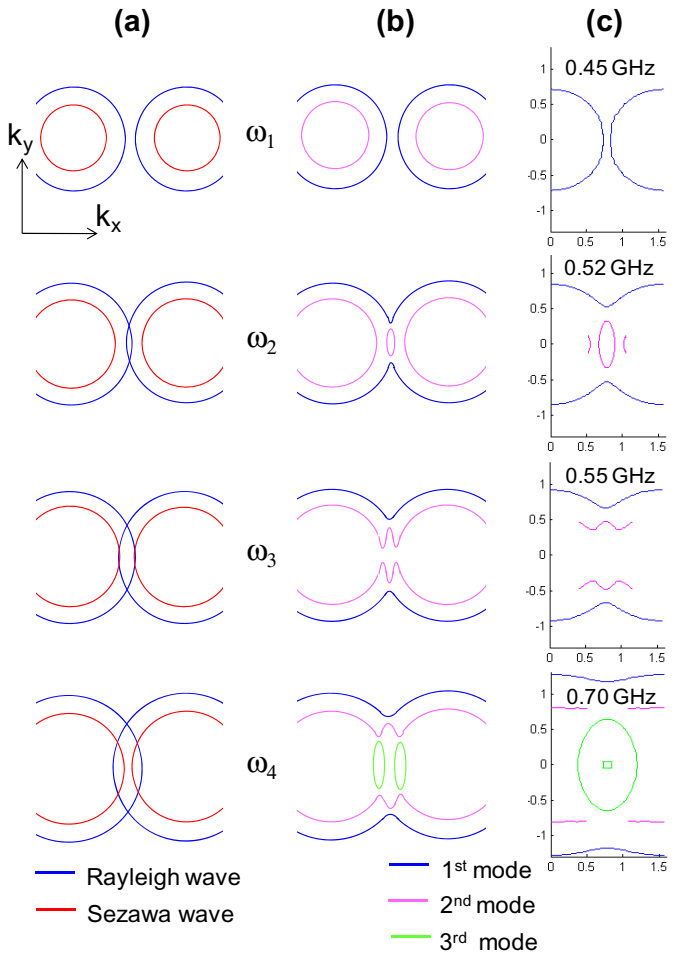

Figure 7. Formation of the dispersion surface of a periodic structure illustrated by horizontal cross-sections of the $\omega(\mathbf{k})$ surface. These approximately correspond to the horizontal dashed lines shown in figure 5. (a) Dispersion cones of the original Rayleigh and Sezawa modes shown schematically in the limit of vanishing periodicity. (b) The formation of the three lowest dispersion sheets of the periodic structure sketched roughly according to the weak perturbation model. (c) Isofrequency cross-sections of the experimentally measured dispersion surface.

4. Conclusions

In conclusion, the laser-induced transient grating technique has been proved well suited for mapping the band structure of an SPC. We have measured dispersion surfaces of the three lowest acoustic modes of a 1D structure comprised of alternating Cu and SiO_2 bars on a Si substrate and explained their formation from the Rayleigh and Sezawa modes of a uniform film/substrate structure. According to the weak-perturbation model, the dispersion surface yields avoided-crossing bandgaps comprised of a saddle below the gap and a parabolic minimum above it. This model has been found to be in agreement with the experimental data for the first and second acoustic dispersion sheets of the structure. However, the shape of the third dispersion sheet

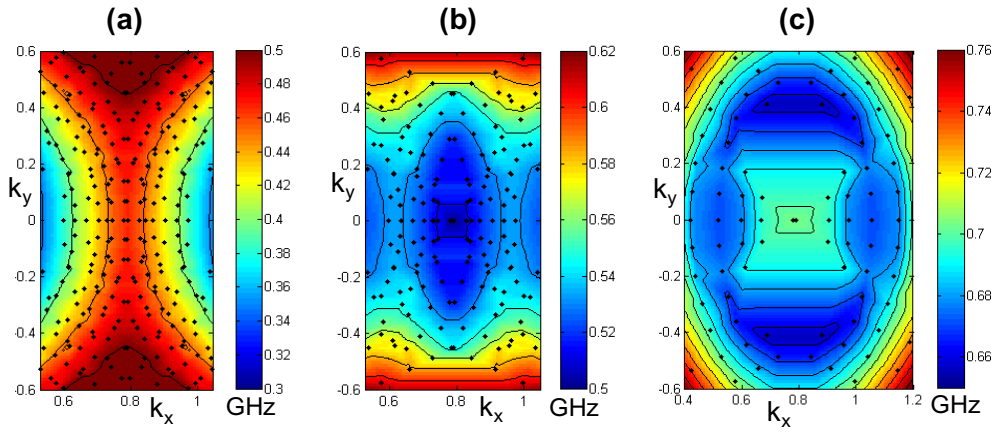

Figure 8. Maps of the central sections of the measured dispersion sheets for the (a) first, (b) second and (c) third modes. Symbols mark the location of the measured points (including those obtained by symmetry transformations). The wavevector components k_x and k_y are expressed in $\mu\mathrm{m}^{-1}$.

defied expectations: in particular, it was shown to contain minima located off the direction of periodicity. An intriguing consequence of this finding is the existence of zero group velocity waves with the wavevector at an angle to the periodicity direction. We believe that mapping the dispersion surfaces of 2D phononic crystals should yield even more interesting results. The approach used in this work may be extended beyond phononic crystals: for example, the transient grating technique has been used to measure the dispersion of phonon-polaritons in $LiNbO_3$ and $LiTaO_3$ [25]; thus it may prove instrumental for studying the band structure of photonic crystals in the THz range fabricated in these materials [26].

Acknowledgments

Donation of the measurement system by Advanced Metrology Systems, LLC, is greatly appreciated. AAM is grateful to A G Every for stimulating discussions. The contribution of AAM was supported, in the data analysis part, by the US Department of Energy, Office of Basic Energy Sciences as part of the S^3TEC Energy Frontier Research Center under award no. DE-SC0001088.

References

[1] Rytov S M 1956 *Akust. Zh.* **2** 71
Rytov S M 1956 *Sov. Phys. Acoust.* **2** 67 (Engl. Transl.)
[2] Datta S 1986 *Surface Acoustic Wave Devices* (Englewood Cliffs, NJ: Prentice-Hall)
[3] Sigalas M, Kushwaha M S and Economou E N 2005 *Z. Kristallogr.* **220** 765
[4] Tanaka Y and Tamura S 1998 *Phys. Rev.* B **58** 7958
[5] Dhar L and Rogers J A 2000 *Appl. Phys. Lett.* **77** 1402
[6] Wu T-T, Wu L-C and Huang Z-G 2005 *J. Appl. Phys.* **97** 094916
[7] Laude V, Wilm M, Benchabane S and Khelif A 2005 *Phys. Rev.* E **71** 036607
[8] Profunser D M, Wright O B and Matsuda O 2006 *Phys. Rev. Lett.* **97** 055502

[9] Robillard J-F, Devos A and Roch-Jeune I 2007 *Phys. Rev.* B **76** 092301
[10] Giannetti C *et al* 2007 *Phys. Rev.* B **76** 125413
[11] Maznev A A 2008 *Phys. Rev.* B **78** 155323
[12] Maznev A A and Wright O B 2009 *J. Appl. Phys.* **105** 123530
[13] Profunser D M, Muramoto E, Matsuda O, Wright O B and Lang U 2009 *Phys. Rev.* B **80** 014301
[14] Dutcher J R, Lee S, Hillebrands B, McLaughlin G J, Nickel B G and Stegeman G I 1992 *Phys. Rev. Lett.* **68** 2464
[15] Lin H, Maris H J, Freund L, Lee K, Luhn H and Kern D 1993 *J. Appl. Phys.* **73** 37
[16] Maznev A A, Mazurenko A, Zhuoyun L and Gostein M 2003 *Rev. Sci. Instrum.* **74** 667
[17] Glass N E and Maradudin A A 1983 *J. Appl. Phys.* **54** 796
[18] Lothe J and Barnett D M 1976 *J. Appl. Phys.* **47** 428
[19] Farnell G W and Adler E L 1972 *Physical Acoustics, Principles and Methods* vol 9, ed W P Mason and R N Thurston (New York: Academic) p 35
[20] Grimsditch M 1985 *Phys. Rev.* B **31** 6818
[21] Zhao J-H, Ryan T, Ho P S, McKerrow A J and Shih W-Y 1999 *J. Appl. Phys.* **85** 6421
[22] Simmons G and Wang H 1971 *Single Crystal Elastic Constants and Calculated Aggregate Properties: A Handbook* (Cambridge, MA: MIT Press)
[23] Maznev A A and Every A G 2009 *J. Appl. Phys.* **106** 113531
[24] Landau L D and Lifshitz E M 1991 *Quantum Mechanics* (Oxford: Butterworth-Heinemann)
[25] Crimmins T F, Stoyanov N S and Nelson K A 2002 *J. Chem. Phys.* **117** 2882
[26] Peier P, Merbold H, Pahinin V, Nelson K A and Feurer T 2010 *New J. Phys.* **12** 013014